A Method of Moments Analysis and a Finite-Difference Time-Domain Analysis of a Probe–Sleeve Fed Rectangular Waveguide Cavity

John M. Jarem, *Member, IEEE*

Abstract—**A multifilament method of moments (MOM) analysis and a finite-difference time-domain (FD–TD) analysis have been used to numerically calculate the input impedance of a probe–sleeve fed rectangular waveguide which has been short-circuited on one side. The input impedance of the system has been determined by using the above methods for several probe–sleeve configurations and reasonable agreement between the two methods for the cases studied has been found. A MOM Green's function formulation which is based on scattering superposition has also been derived which allows the input impedance of a probe–sleeve feed to be calculated when the waveguide is terminated in a given load. The MOM results and FD–TD numerical results are compared for this loaded waveguide input impedance case and reasonable agreement between the methods has been found. A comparison of theory and experiment is given when the waveguide is terminated in a ground plane aperture.**

I. Introduction

An important problem in the microwave area is determining the input impedance of a probe feed when it is placed in a rectangular waveguide which is short-circuited on one side and terminated with a waveguide load on the other side. This probe input impedance problem has important applications for the design of cavity-backed slot antennas for aircraft or missiles when the terminating waveguide load is an aperture which radiates into free space or some other dielectric medium (for example, a missile plasma sheath layer) and has important applications for the design of microwave circuits.

A limitation of exciting a semi-infinite waveguide only by a single probe is the fact that only the probe height h and the short circuit distance d (See Fig. 1) can be used to tune the probe for maximum power transfer. A way of overcoming this problem is to add a metallic sleeve to the waveguide, either above the probe or to the side of the probe. The addition of the sleeve can cause a large change in the input impedance of the system, depending on the probe's and the sleeve's size and position and on the load which is used as a waveguide termination. For the above-described reason, then, the determination of the input impedance of the probe–sleeve feed system is an important problem to solve as the addition of the metallic sleeve gives the microwave designer additional parameters (sleeve length and position) with which to tune and match the input impedance of the overall rectangular waveguide system.

Manuscript received March 21, 1990; revised November 13, 1990.

The author is with the Department of Electrical and Computer Engineering, University of Alabama in Huntsville, Huntsville, AL 35899.

IEEE Log Number 9042349.

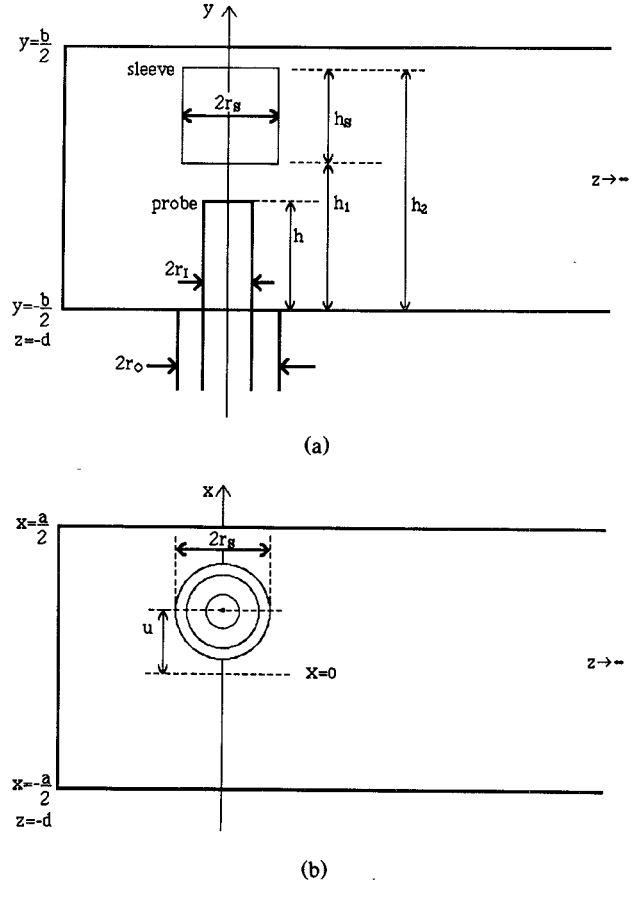

Fig. 1. The geometry of the probe–sleeve waveguide system is shown when a semi-infinite waveguide terminates the waveguide system. (a) Side view. (b) Top view.

The problem of determining the input impedance of a probe inside a waveguide has been analyzed by many authors, including Collin [1], who derived a variational expression for the input impedance of a probe inside a waveguide, Williamson [2]–[7] and Rollins *et al.* [8], who used a combination Fourier transform and MOM approach to determine the input impedance of a probe inside of a waveguide, and

0018-9480/91/0300-0444$01.00 ©1991 IEEE

Jarem [9] and Helaly and Jarem [10], who used a multifilament MOM approach to analyze the probe impedance waveguide problem. Very recently McLeod [11] has used the finite-difference time-domain (FD–TD) method to analyze the electromagnetic fields in a waveguide.

The purpose of the present paper will be to analyze the above-described metallic probe–sleeve waveguide feed system and determine to what extent a sleeve affects the input impedance of a loaded rectangular waveguide system. The analysis will be carried out by using a multifilament MOM approach as was done in [9] and will also be performed by using a FD–TD approach. The two approaches are used in order to validate to some extent the results of each method. A comparison of data collected by the MOM approach, the FD–TD approach, and experiment will also be given.

II. Method of Moments, Multifilament Analysis

This section will be concerned with presenting a method of moments, multifilament analysis of the electric fields and currents in a probe–sleeve fed rectangular waveguide. The analysis is based on (1) using Green's function to calculate the electric fields which radiate from all currents and sources in the waveguide, (2) imposing boundary conditions on the electric field at the appropriate perfect conductor surfaces in the waveguide (metallic probe and sleeve surfaces), and (3) using the method of moments to solve the resulting electric field integral equations which result. The input impedance is calculated from the method of moments solution by dividing the net probe current at the base of the probe into the coaxial voltage potential difference at the base of the probe.

The Green's functions which describe electric fields which radiate in the waveguide and which are used to define the electric field integral equation consist of (1) the Green's function which describes the radiation from magnetic surface current at the base of the coaxial cable to the probe sleeve surface, (2) the Green's function which describes the radiation that arises from electric surface current on the probe–sleeve surface back onto itself, and (3) the Green's function which describes radiation from electric surface current on the probe sleeve surface when a waveguide load reflects energy back into the waveguide probe feed system.

Mathematically the boundary conditions and electric fields which define the equations for the probe and sleeve currents in a loaded waveguide at the probe or sleeve surface are given by the equations

$$E_y^J + E_y^A = -E_y^M \tag{1}$$

where

$$E_y^J = \int_{\text{P.S.}} G_{yy}^J(x,y,z|x',y',z') \cdot J_y(x',y',z') r(x',z')\, d\varphi'\, dy' \tag{2}$$

where

$$G_{yy}^J = \frac{-j\eta}{k}\frac{4Il}{ab}\sum_{\substack{m=1\\n=0}}^{\infty}\frac{1}{\gamma\bar{\epsilon}_n}\left(-k_y^2+k^2\right)S_xC_yS_{x'}C_{y'}f(z,z')$$

where

$$f(z,z') = \begin{cases} e^{-\gamma(z'+d)}\sinh\gamma(z+d), & z<z' \\ e^{-\gamma(z+d)}\sinh\gamma(z'+d), & z>z' \end{cases}$$

$$S_xC_yS_{x'}C_{y'} = \sin k_x\left(x+\frac{a}{2}\right)\cos k_y\left(y+\frac{b}{2}\right) \cdot \sin k_x\left(x'+\frac{a}{2}\right)\cos k_y\left(y'+\frac{b}{2}\right)$$

$$k_x = \frac{m\pi}{a} \qquad k_y = \frac{n\pi}{b}$$

$$\bar{\epsilon}_n = \begin{cases} 2, & n=0 \\ 1, & n\neq 0 \end{cases} \qquad \gamma = \left[k_x^2+k_y^2-k^2\right]^{1/2}$$

$$\eta = \sqrt{\frac{\mu}{\epsilon}} \qquad k = \omega\sqrt{\mu\epsilon} \qquad Il = 1\ (\text{A}\cdot\text{m})$$

where

$$E_y^A = \int_{\text{P.S.}} G_{yy}^A J_y r\, d\varphi'\, dy'$$

$$G_{yy}^A = \frac{\Gamma}{1+\Gamma e^{-j2\beta c}}\left(\frac{4\eta k}{ab\beta}\right)e^{-j2\beta c}\cdot\sin\beta(z'+d)\sin\beta(z+d) \cdot\sin\frac{\pi}{a}\left(x'+\frac{a}{2}\right)\sin\frac{\pi}{a}\left(x+\frac{a}{2}\right)$$

$$\beta = \left(k^2-\left(\frac{\pi}{a}\right)^2\right)^{1/2}.$$

E_y^M is the impressed electric field which arises from the base of the coaxial probe (see [9]) and radiates onto the probe–sleeve surface. In the above expressions $J_y(x',y',z')$ represents the surface current which is on the probe or sleeve, r is the radius of the probe or sleeve, and the dimensions a, b, c, and d are shown in Fig. 2. In (3) the G_{yy}^A Green's function has been derived by assuming that only a TE_{10} mode can propagate in the waveguide and that the waveguide load is far enough away from the probe–sleeve system that higher order modes do not contribute to the input impedance. This in practice is a very good assumption unless the load is very close to the feed system. The G_{yy}^A term has been derived by using scattering superposition; that is, it has been derived by adding the infinite number of forward and backward TE_{10} mode reflections off the short circuit plate and waveguide load that a current element would radiate inside the waveguide. By locating the current element at a point x',y',z' in Fig. 2 and observing the electric field at x,y,z, the Green's function given by (3) is derived. As can be seen from this equation, when $\Gamma = 0$ (no waveguide load), G_{yy}^A is zero, as it should be.

The G_{yy}^J term is based on adding an infinite number of TE_{mn} and TM_{mn} rectangular waveguide modes [1] together to form a slowly converging infinite series over the integers m and n. This series represents the Green's function of a y-directed electric dipole located at (x',y',z') which radiates an E_y electric field to the point (x,y,z). The Green's function given in (2), because it is a slowly converging series, has been converted to a rapidly converging one through the use of a Poisson summation [1], [9]. Discussions of both the slowly converging and the rapidly converging series are given

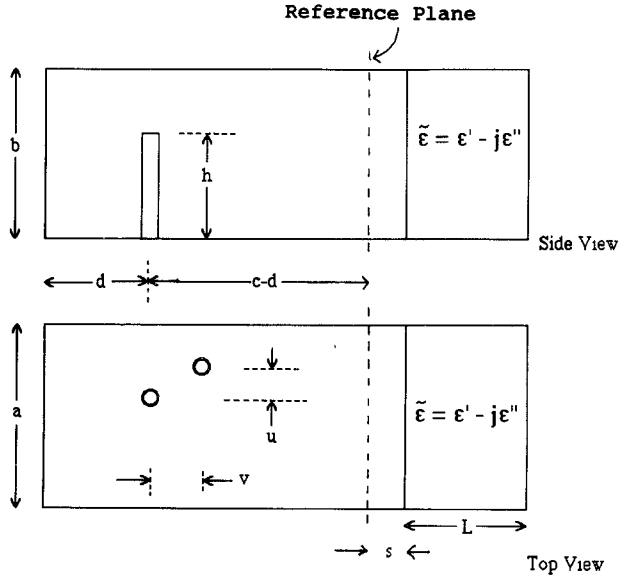

Fig. 2. The geometry of the probe–sleeve waveguide system is shown when a TE_{10} load terminates the waveguide system at a distance of $c-d$ from the probe.

in [9]. The rapidly converging series has been used for all calculations in this paper.

Once the electric field integral equations for the currents on the probe surface and the sleeve surface have been defined, an important problem that remains is to convert this equation into a matrix equation which can then be solved numerically. Several options exist for performing the matrix conversion, depending on the expansion functions which are used to represent the unknown probe and sleeve surface currents and on the testing functions which are used to enforce boundary conditions on the probe and sleeve surfaces. Some examples of the two-dimensional expansion functions that can be used to represent the surface currents of the probe and sleeve are pulse functions in the φ' and y' directions, point-sampled functions in the φ' direction (also called multifilament functions) and wavenumber-dependent entire domain modal functions in the y' direction, and point-sampled functions in the φ' direction and piecewise sinusoidal functions in the y' direction.

In using the above combinations of testing and expansion functions it is important to correctly represent the radius of the probe or sleeve in the system of equations; it is also important to keep the matrix size of the system as small as possible. The use of delta functions (or, equivalently, multifilaments) as expansion and testing functions in the φ and φ' directions and of wave-dependent modal functions as expansion and testing functions in the y and y' directions solves the problem adequately including the probe radius and sleeve radius dimensions in the system of equations but unfortunately also leads to a matrix equation which is relatively large for the type of problem being solved (number of filaments × number of entire domain model functions). It also leads to a matrix equation which is very ill conditioned. The ill conditioning is due to the fact that when matrix elements are delta function sampled around the probe and the sleeve in the φ and φ' directions, the matrix elements which belong to the same group of sampled φ and φ' points tend to be very close together in value and thus form a system of linear equations where many of the equations are very nearly linearly dependent on one another and thereby form an overall set of equations which are ill conditioned.

The present author has found that a simple way to avoid this problem and also provide a matrix equation which is relatively small (4×4) is simply to average the multifilament matrix equation elements over the φ and φ' sampled points and then to solve for the total amount of net current which flows on the probe or sleeve surface (this is $2\pi r$ times the average surface current around the probe or sleeve). The sampling at φ and φ' points around the probe and sleeve is, of course, numerically equivalent to integrating the electric field integral equations around the probe or sleeve surfaces.

The reduced matrix equation that results from the procedure described above is given by

$$\sum_{p'=1}^{P_T'} \sum_{s_{p'}'=1}^{S_{p'T}'} I_{s_{p'}'} \left\{ \frac{1}{N_f^2} \sum_{i_p=1}^{N_f} \sum_{i_{p'}=1}^{N_f} \cdot \int_{\mathrm{PL}_{tp}} \int_{\mathrm{PL}_{ep'}} t_{s_p}(y) G_{yyi_p,i_{p'}} t_{s_{p'}'}(y')\, dy\, dy' \right\} = -\sum_{p=1}^{P_T} E_y^I t_{s_p}(y)\, dy,$$

$$S_p = 1, \cdots, S_{p_T};\ p = 1, \cdots, P_T. \tag{4}$$

In the above expressions the integrals over PL_{tp} and $\mathrm{PL}_{ep'}$ represents a y or y' integration over the length of the probe or sleeve for which a test or expansion function is being integrated over. In the above expressions i_p and $i_{p'}'$ represent the points around the probe and sleeve where the φ and φ' coordinates have been sampled. The φ and φ' coordinates have been displaced from one another by $\Delta\varphi/2$, where $\Delta\varphi = 2\pi/N_f$, in order to maximize the separation between source and observation points, which in turn guarantees maximum convergence of the series solutions. The integers $S_{p'_T}'$ and S_{p_T} represent the number of modal functions which are used as expansion or testing functions on the probe or sleeve surface.

The $t_{s_p}(y)$ and $t_{s_{p'}'}(y')$ functions have been chosen as wave-dependent entire domain functions. The choice of modal functions in the y direction is an important one and can be used to impose the condition whether the probe or sleeve currents vanish or do not vanish at the probe or sleeve tips. In this paper, in order to impose a Galerkin procedure, the testing functions for the same probe length have always been chosen the same as the expansion functions. The expansion and testing functions which have been used in this paper for the probe are all linear combinations of $\sin k(h-(y+b/2))$, $1-\cos k(h-(y+b/2))$, $\sin ky$, $\cos ky$, and $\sin[(\pi/(h_2-h_1))\ (y-h_1)]$. The last function is the only non-wave-dependent entire domain included in the analysis. It has been included because it causes the current at an isolated sleeve to vanish at the sleeve tips. Linear combinations of the above functions can be used to cause the electric current to vanish or not vanish at the probe's end or the sleeve's end. The wave-dependent modal functions were first suggested by Collin [1] and seem to produce very reliable impedance results when used.

III. Finite-Difference Time-Domain Analysis

An alternative method of numerically calculating the electric currents, fields, and input impedance of a probe–sleeve fed waveguide is provided by the FD–TD algorithm. This

algorithm calculates the electromagnetic fields and currents in the waveguide by using the finite differences to numerically solve Maxwell's equations in the probe–sleeve waveguide environment. In this method all spatial and temporal derivatives are approximated by finite differences in a three-dimensional grid. These finite differences are substituted into Maxwell's equations and then manipulated in such a way that past and present values of the electric and magnetic fields can be marched forward in time to predict new values of the electric and magnetic fields. This method has been used to solve a wide variety of electromagnetic problems, including scattering from lossy dielectric bodies, scattering from aircraft, microwave absorption of energy in the body, and the analysis of patch antennas. Reference [12] gives a review of the method. McLeod [11] has recently determined the input impedance of a waveguide by using this method.

In this paper the input impedance of the waveguide probe–sleeve feed system has been calculated by the FD–TD method through a recently developed computer program called TSARS (Temporal Scattering and Reflectance Software) [13], [14]. In the present application the input impedance was calculated by placing a sinusoidal gap voltage source at the base of the probe feed, calculating numerically the sinusoidal current that flowed at the base of the probe feed, converting the time-domain sinusoidal solutions to phasor form, and then taking the ratio of the two phasor quantities to find the input impedance of the system. The current flowing at the base of the probe was found by calculating

$$I = \oint \vec{H} \cdot d\vec{l}$$

around the wire. All computer runs were made for a long enough time to ensure steady-state conditions. The probe and metallic sleeve were both modeled numerically using the thin-wire approximation derived by Taflove *et al.* in [15].

Nonzero waveguide load conditions which could produce a reflection coefficient

$$\Gamma = |\Gamma| e^{j\varphi}$$

were simulated numerically by placing at the end of the waveguide (the reference plane of Fig. 2), at a distance S from the reference plane, a lossy dielectric of relative dielectric value $\tilde{\epsilon}_R = \epsilon' - j\epsilon''$ of length L. (See Fig. 2.) A short calculation shows that the TE_{10} reflection coefficient Γ from this load is given by

$$\Gamma = \frac{R-1}{R+1} e^{-j2\beta' S} \tag{5}$$

where

$$R = \frac{j\beta'}{\gamma'} \tan k\gamma' k_0 L$$

$$\beta' = \left[1 - \left(\frac{\lambda}{2a}\right)^2\right]^{1/2} \qquad \gamma' = \left[\left(\frac{\lambda}{2a}\right)^2 - (\epsilon' - j\epsilon'')\right]^{1/2}$$

$$k_0 = \frac{2\pi}{\lambda} \qquad \lambda = \text{free-space wavelength.}$$

By adjusting ϵ', ϵ'', L, and S at a single frequency ω, virtually any reflection coefficient Γ can be simulated. Numerical runs using the FD–TD algorithm verified the above TE_{10} reflection coefficient formulas to within a few percent (2 to 3%).

Although (5) can be used to calculate the case where $\Gamma = 0$, an alternative method was used to simulate conditions of a matched waveguide load (that is, a waveguide section which is semi-infinite to the right) being present. This alternative method consisted in building a very long FD–TD waveguide grid and exciting this grid at $t = 0$ for enough time periods for the probe–sleeve system to be in steady state locally near the probe–sleeve short circuit wall (approximately five time periods). However, the number of time periods must be kept low enough so that the TE_{10} mode of the waveguide does not have time to return to the probe–sleeve system to interfere electromagnetically with that system. In this way a very accurate simulation of a semi-infinite waveguide load condition can be produced. With this method, a more accurate $\Gamma = 0$ load condition could be imposed than by the use of the load described by (5).

IV. Numerical Results

The validity of the MOM and FD–TD methods for determining antenna input impedance was tested by calculating the input impedance (normalized to 50 Ω) of a loaded semi-infinite waveguide antenna and then comparing the numerical results with experimental data. The validity of the method was also tested numerically by directly comparing MOM and FD–TD results when a few different probe–sleeve geometries were used to excite the semi-infinite waveguide system.

Fig. 3 shows the input impedance (normalized to 50 Ω) of a centered, probe-excited cavity aperture antenna (see Fig. 3 inset) as determined by experiment (square), MOM (triangle), and FD–TD (diamond) when the cavity dimensions are $a = 2.246$ in., $b = 1.133$ in., $c = 1.984$ in., $d = 0.758$ in., and $h = 0.5665$ in. and when the frequency is varied from 3 GHz (which is above the TE_{10} cutoff frequency of 2.63 GHz) to 5 GHz (which is below the next highest modal cutoff frequency of 5.21 GHz). The input impedance of the antenna including the modification of the impedance due to the presence of a waveguide ground plane aperture termination (see Fig. 3 inset) was determined by calculating the waveguide reflection coefficient Γ associated with the aperture (from the theory of [16]), using these values of Γ in (3) (when calculating Z_{IN} from the MOM) or (5) (when calculating Z_{IN} from the FD–TD method) and then following the theory previously described in Sections II and III to complete the analysis. The waveguide reflection coefficients which were used were $\Gamma = 0.18\angle -86°$ (at 3 GHz), $\Gamma = 0.21\angle -84°$ (at 4 GHz), and $\Gamma = 0.17\angle -90°$ (at 5 GHz). In Fig. 3, the upper three curves represent the real part of the input impedance (normalized to 50 Ω) and the lower three curves represent the imaginary part of the input impedance (normalized to 50 Ω). As can be seen, good agreement exists between theory (MOM and FD–TD) and experiment, with the MOM approach clearly giving consistently more accurate results than the FD–TD method. It is interesting that the experimental data seem to be bracketed by the MOM and FD–TD results.

Fig. 4 shows the input impedance of a center-fed probe with no sleeve present when the probe height varies from $0.3b$ to $1.0b$ at a frequency of 4.0 GHz. The waveguide dimensions are given in the inset. As can be seen, good

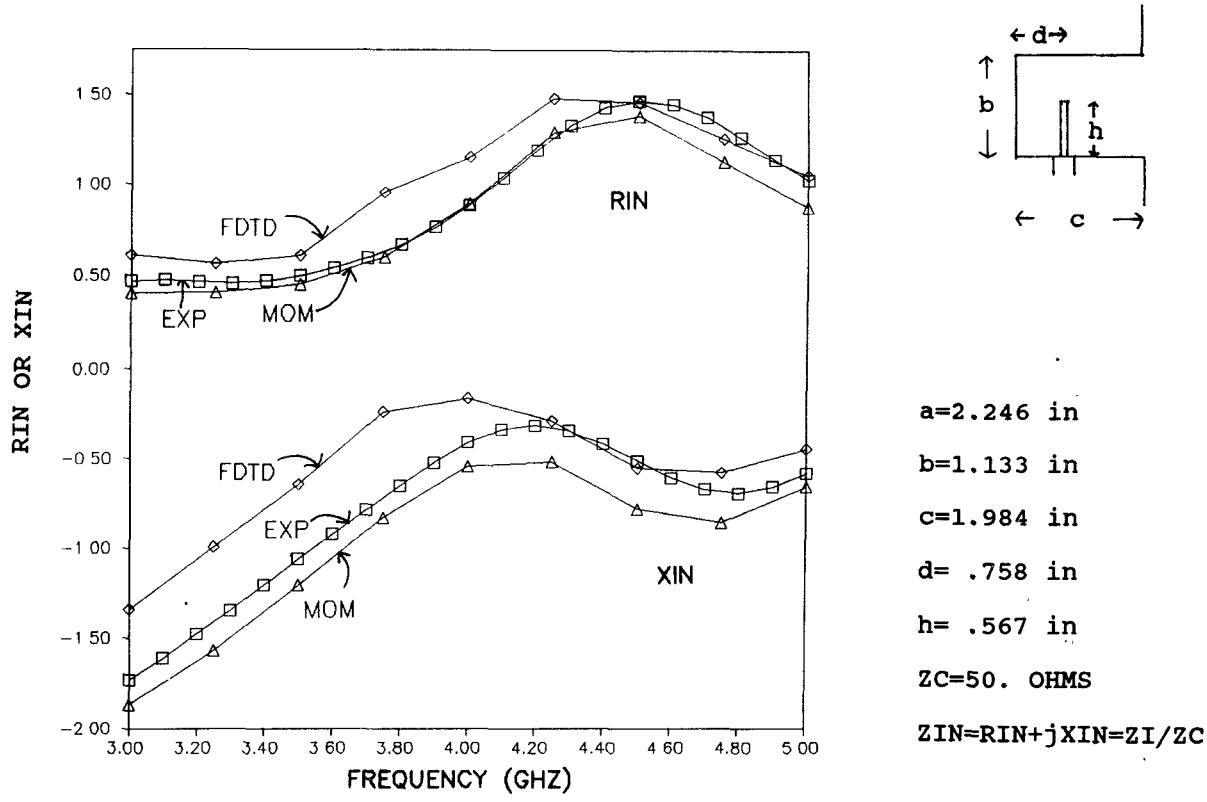

Fig. 3. The real (upper curves) and imaginary (lower curves) parts of the normalized input impedance of a cavity-aperture antenna are shown as determined by experiment, by the MOM approach, and by the FD–TD approach.

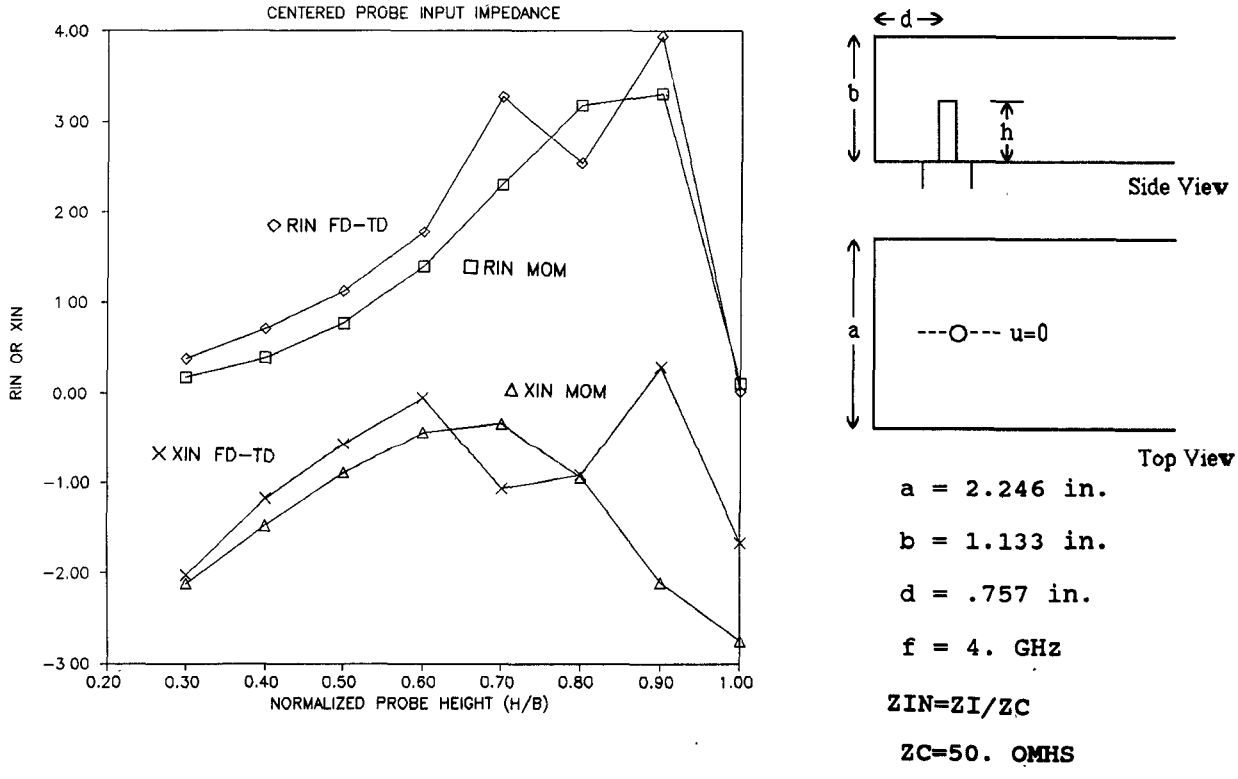

Fig. 4. The real and imaginary parts of the input impedance as determined by MOM and FD–TD are shown when the probe is centered ($u = 0$) and when the probe height varies from $0.3b$ to $1.0b$.

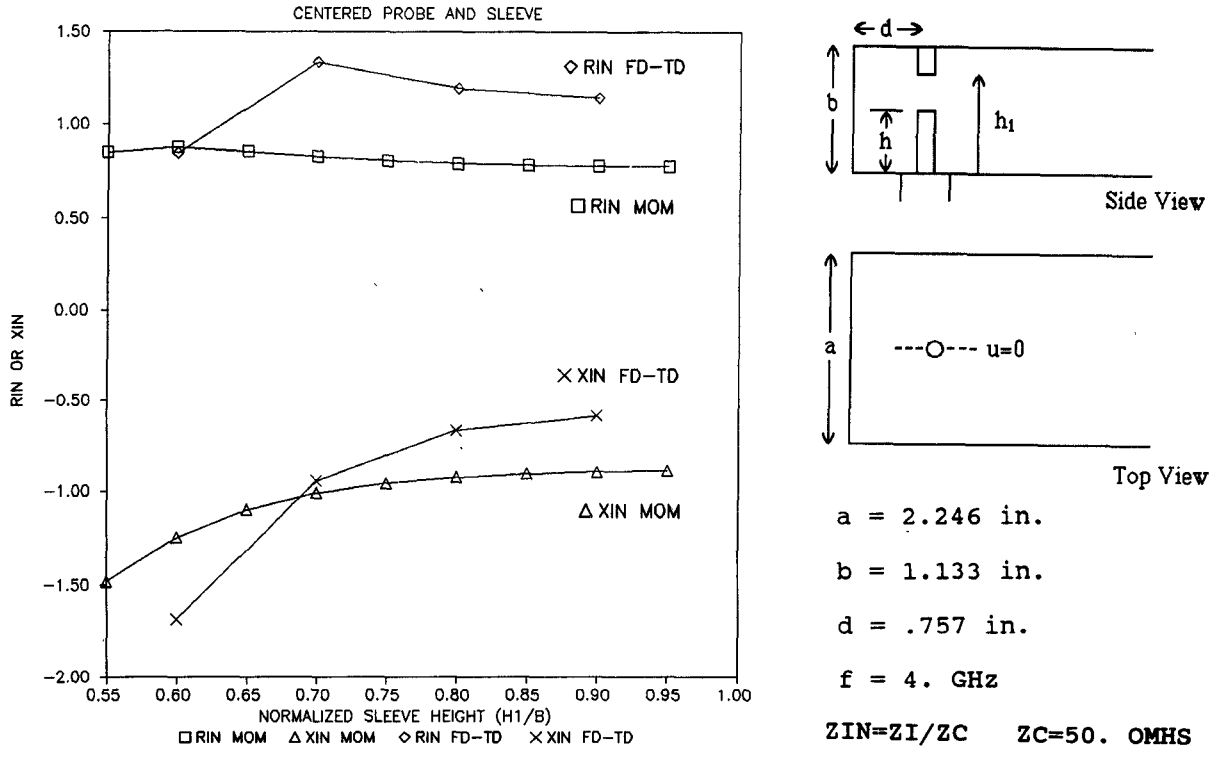

Fig. 5. The real and imaginary parts of the input impedance as determined by MOM and FD–TD are shown when a probe of height $h = 0.5b$ is placed in the waveguide and centered. A sleeve which is attached to the waveguide top wall is placed directly above the probe ($u = 0$, $v = 0$). In this figure the bottom of the sleeve varies from $h_1 = 0.55b$ to $h_1 = 0.95b$.

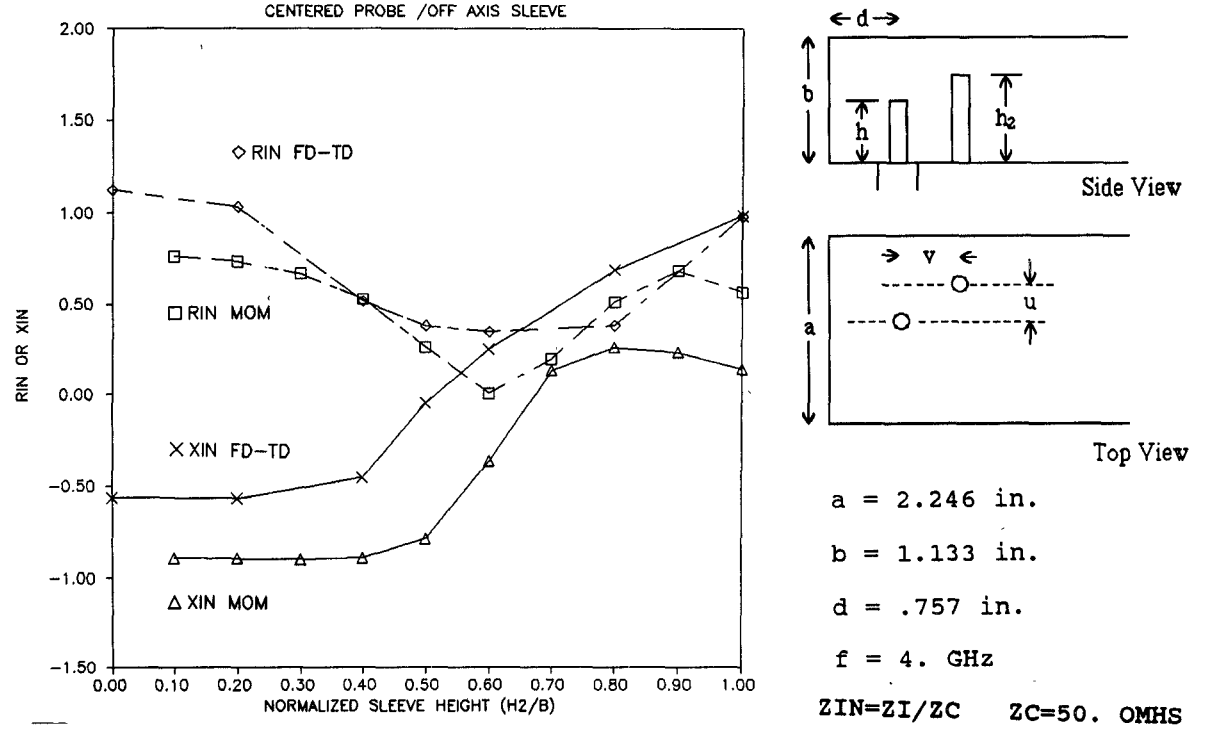

Fig. 6. The same input impedance case as described in Fig. 5 is shown in this figure except that the sleeve is attached to the bottom waveguide wall ($h_1 = 0$) and the upper sleeve height varies from $h_2 = 0$ (no sleeve present) to $h_2 = b$. The sleeve is located at $u = 0.15a$ and $v = 0.2a$.

agreement exist between the two methods except for the calculation of the reactance X (the imaginary part of normalized input impedance) when $h = 0.9b$. The author believes that the discrepancy occurs at this point because only a single grid cell models the gap between the probe tip and the top of the waveguide wall using the FD–TD method. It is interesting to note that the MOM impedance results seem to almost average the FD–TD results.

Fig. 5 shows the input impedance of the probe–sleeve system when a centered probe of height $h = 0.5b$ is placed in the waveguide and when a sleeve which is attached to the top waveguide wall is placed directly above the probe. The bottom of the sleeve varies from a position of $0.55b$ up to $0.95b$. As can be seen, fair agreement exists between the two methods in Fig. 5. It is interesting and important to note that both methods in Fig. 5 show the same general trends in impedance change as the sleeve length changes.

Fig. 6 shows the case where a centered probe $h = 0.5b$ is placed in the waveguide and an off-axis sleeve which is attached to the waveguide bottom wall is placed $0.15a$ to the side of the probe and $0.2a$ forward of the sleeve. As can be seen, although close agreement does not exist between the MOM and FD–TD methods, both methods are showing very similar trends in the change of impedance with sleeve height.

A difference (or error) analysis of the data presented in Figs. 3–6 has been prepared in order to quantitatively gauge the performance of the MOM and FD–TD methods relative to experiment and to each other. The difference analysis is performed by first calculating the coaxial cable reflection coefficients which are associated with the two sets of input impedance data which are to be compared, subtracting the reflection coefficients, and then squaring and averaging the magnitude of the complex reflection coefficient difference in an appropriate manner. The numerical difference between the reflection coefficients associated with any two sets of impedance data (either numerical or experimental) was computed by the following formula:

$$\epsilon = \left(\frac{1}{N} \sum_{i=1}^{N} |\Gamma_{i1} - \Gamma_{i2}|^2 \right)^{1/2} \Big/ 2 \qquad (6)$$

where

$$\Gamma_{ij} = \frac{Z_{\mathrm{IN}_{ij}} - 1}{Z_{\mathrm{IN}_{ij}} + 1}, \qquad i = 1, \cdots, N;\ j = 1, 2$$

where $Z_{\mathrm{IN}_{ij}}$ = the normalized input impedance for which an error analysis is to be performed and N is the number of points over which the average error is to be computed. Equation (6) has been normalized by dividing the rms difference by its maximum possible value, which is 2. Based on (6), we will now give the reflection coefficient rms differences of Figs. 3–6. The average RMS difference between the MOM impedance data of Fig. 3 and the experimental data was 3.93%, and the average rms difference between the FD–TD data of Fig. 3 and the experimental data was 9.20%. As can be seen from these values, the MOM analysis was more accurate than the FD–TD data for this case. The average rms difference errors as computed by (6) for the FD–TD and MOM impedance data for Figs. 4–6 were 10.3%, 9.74%, and 25.0% respectively.

Based on the results of comparing the experimental data, the MOM data, and the FD–TD numerical data, the author feels that the MOM data represent a more accurate method of calculating input impedance than the FD–TD method. The author feels, however, that the best overall numerical results are obtained when the two methods are used together to validate each other.

V. Summary

A multifilament method of moments (MOM) analysis and a finite-difference time-domain (FD–TD) analysis have been used to numerically calculate the input impedance of a probe–sleeve fed rectangular waveguide. The input impedance of the probe for several probe–sleeve configurations using the above methods has been calculated and reasonable agreement between the two methods for the cases studied has been found. Comparison of theory and experiment shows that the MOM and FD–TD numerical methods both agree acceptably well with experimental data.

Acknowledgment

The author would like to thank W. Schaedla and B. Brock for their helpful comments and advice on the present paper. Thanks are also due to A. Helaly for the numerical analysis that he performed in this paper.

References

[1] R. E. Collins, *Field Theory of Guided Waves*. New York: McGraw-Hill, 1960, pp. 258–271.

[2] A. G. Williamson and D. V. Otto, "Coaxially fed hollow cylindrical monopole in a rectangular waveguide," *Electron Lett.*, vol. 9, no. 10, pp. 218–220, May 17, 1973.

[3] A. G. Williamson, "Coaxially fed hollow probe in a rectangular waveguide," *Proc. Inst. Elec. Eng.*, vol. 132, part H, pp. 273–285, 1985.

[4] A. G. Williamson and D. V. Otto, "Cylindrical antenna in a rectangular waveguide driven from a coaxial line," *Electron. Lett.*, vol. 8, no. 22, pp. 545–547, Nov. 2, 1972.

[5] A. G. Williamson, "Equivalent circuit for radial-line/coaxial-line junction," *Electron. Lett.*, vol. 17, no. 8, pp. 300–301, Apr. 16, 1981.

[6] A. G. Williamson, "Analysis and modelling of a coaxial-line/rectangular-waveguide junction," *Proc. Inst. Elec. Eng.*, vol. 129, part H, no. 5, pp. 262–270, Oct. 1982.

[7] A. G. Williamson, "Radial line/coaxial-line junctions: Analysis and equivalent circuits," *Int. J. Electron.*, vol. 58, pp. 91–104, 1985.

[8] J. M. Rollins and J. M. Jarem, "The input impedance of a hollow-probe-fed, semi-infinite rectangular waveguide," *IEEE Trans. Microwave Theory Tech.*, vol. 37, pp. 1144–1146, July 1989.

[9] J. M. Jarem, "A multifilament method-of-moments solution for the input impedance of a probe-excited semi-infinite waveguide," *IEEE Trans. Microwave Theory Tech.*, vol. MTT-35, pp. 14–19, Jan. 1987.

[10] A. Helaly and J. Jarem, "Input impedance of a probe excited semi-infinite rectangular waveguide with a tuning post," in *Proc. 22nd Southeastern Symp. System Theory* (Cookeville, TN), Mar. 11–13, 1990, pp. 161–167.

[11] R. R. McLeod, S. T. Pennock, and M. J. Barth, "Time-domain analysis of wave-guide fed antennas," in *Proc. 1989 URSI Rad. Sci. Mtg.*, June 26–30, 1989, p. 269.

[12] A. Taflove and K. R. Umashanker, "Finite-difference time-domain (FD–TD) modeling of electromagnetic wave scattering and interaction problems," *IEEE Antennas Propagat. Soc. Lett.*, vol. 30, no. 2, pp. 5–20, Apr. 1988.

[13] S. L. Ray, "Electromagnetic finite-difference time-domain (FD–TD) modeling II: Details of the method," Lawrence Livermore National Laboratory, Livermore, CA., 94550, Apr. 1989.

[14] R. R. McLeod, "Temporal scattering and reflection software," Users Manual, Lawrence Livermore National Laboratories, Livermore, CA., 94550, Sept. 1987.

[15] A. Taflove, K. R. Umashankar, B. Beker, and F. Harfoush, "Detailed FD–TD analysis of electromagnetic fields penetrat-

ing narrow slots and lapped joints in thick conducting screens," *IEEE Trans. Antennas Propagat.*, vol. 36, pp. 247–257, Feb. 1988.

[16] K. E. Golden and G. E. Stewart, "Self and mutual admittances of rectangular slot antennas in the presence of an inhomogeneous plasma layer," *IEEE Trans. Antennas Propagat.*, vol. AP-17, pp. 763–771, Nov. 1969.

✠

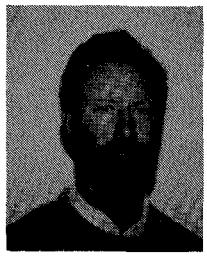

John M. Jarem (M'82) was born in Monterey, CA, on May 10, 1948. He received the B.S., M.S. and Ph.D. degrees in electrical engineering from Drexel University, Philadelphia, PA, in 1971, 1972, and 1975, respectively.

From 1975 to 1981 he worked as an Assistant Professor of Electrical Engineering at the University of Petroleum and Minerals, Dhahran, Saudi Arabia. He was with the University of Texas at El Paso as an Associate Professor of Electrical Engineering from 1981 to 1987, and he has been a Professor of Electrical Engineering at the University of Alabama, Huntsville, since 1987. His research interests are electromagnetics and antenna theory.